HHS Public Access

Author manuscript

Neuron. Author manuscript; available in PMC 2020 June 19.

Published in final edited form as:

Neuron. 2019 June 19; 102(6): 1223–1234.e4. doi:10.1016/j.neuron.2019.04.001.

VIP interneurons contribute to avoidance behavior by regulating information flow across hippocampal-prefrontal networks

Anthony T. Lee[1], **Margaret M. Cunniff**[1], **Jermyn Z. See**[1], **Scott A. Wilke**[1], **Francisco J. Luongo**[1], **Ian T. Ellwood**[1,2], **Srimadh Ponnavolu**[1], **Vikaas S. Sohal**[1,3,*]

[1]Department of Psychiatry, Weill Institute for Neuroscience, Kavli Institute for Fundamental Neuroscience, and Sloan-Swartz Center for Theoretical Neurobiology, University of California, San Francisco, 675 Nelson Rising Lane, San Francisco, CA 94143-0444

[2]Present address: Department of Neurobiology and Behavior, Cornell University, Ithaca, NY 14853

[3]Lead contact: Vikaas Sohal, Vikaas.Sohal@ucsf.edu

SUMMARY

Inhibitory interneurons expressing vasoactive intestinal polypeptide (VIP) are known to disinhibit cortical neurons. However, it is unclear how disinhibition, occurring at the single-cell level, interacts with network-level patterns of activity to shape complex behaviors. To address this, we examined the role of prefrontal VIP interneurons in a widely-studied mouse behavior: deciding whether to explore or avoid the open arms of an elevated plus maze. VIP interneuron activity increases in the open arms and disinhibits prefrontal responses to hippocampal inputs, which are known to transmit signals related to open arm avoidance. Indeed, inhibiting VIP interneurons disrupts network-level representations of the open arms, and decreases open arm avoidance specifically when hippocampal-prefrontal theta synchrony is strong. Thus, VIP interneurons effectively gate the ability of hippocampal input to generate prefrontal representations which drive avoidance behavior. This shows how VIP interneurons enable cortical circuits to integrate specific inputs into network-level representations that guide complex behaviors.

eTOC blurb

How VIP interneurons modulate network-level activity to regulate behavior is not understood. Lee et al. show that in the elevated plus maze, prefrontal VIP neurons promote open arm avoidance by

*Corresponding author: Vikaas.Sohal@ucsf.edu, University of California, San Francisco, 675 Nelson Rising Lane, San Francisco, CA 94143-0444.

AUTHOR CONTRIBUTIONS

AL and MC performed the experiments and analyzed the data. SW helped with data collection, and JS, FL, IE, SP, and VS all contributed to analysis. AL and VS designed the study and wrote the manuscript.

DECLARATION OF INTERESTS

The authors declare that they have no competing financial interests.

disinhibiting theta-frequency communication that transmits anxiety-related information across hippocampal-prefrontal networks.

INTRODUCTION

Specific neuronal classes alter activity in individual downstream neurons in ways that are now beginning to be understood. However, understanding how these actions on single cells interact with network-level representations of behavioral information remains unclear. For example, in neocortex, GABAergic interneurons which express vasoactive intestinal polypeptide (VIP) are known to mainly inhibit other classes of GABAergic interneurons (Lee et al., 2013; Pfeffer et al., 2013; Pi et al., 2013). Through this action, VIP interneurons disinhibit the responses of cortical excitatory neurons to various stimuli (Ayzenshtat et al., 2016; Fu et al., 2014; Karnani et al., 2016; Pi et al., 2013), altering both network activity and behavior (Kamigaki and Dan, 2017). However, there are many outstanding questions about the relationship between VIP interneurons, network activity, and behavior. First, can we identify specific patterns of network activity which link VIP interneurons to their behavioral effects? In particular, can we show that changes in VIP interneuron activity alter specific patterns of network activity, such that the degree of alteration predicts the magnitude of accompanying changes in behavior? Second, do the behavioral effects of manipulating VIP interneurons depend on the current state of the network and its inputs? For example, if an input is known to drive a behavior, does manipulating VIP neurons exert a consistent effect on that behavior regardless of whether that input is strong or weak? Questions like these highlight critical gaps in our current understanding of exactly how network activity mediates and modulates the behavioral effects of activity in a specific neuronal population.

To address these questions, we studied the role of VIP interneurons within the medial prefrontal cortex (mPFC) in a commonly studied behavior: open arm avoidance in the elevated plus maze (EPM). The EPM comprises two exposed open arms and two closed arms surrounded by high walls, which elicit ethologically-relevant avoidance behavior that reflects the innate preference of mice for the safety of closed spaces over open ones. We first show a role for prefrontal VIP interneurons in open arm avoidance. Then we show that VIP interneurons contribute to network-level representations of the open arms. When we inhibit prefrontal VIP interneurons, the amount by which these representations change predicts the change in open arm avoidance. Prefrontal open arm representations are known to be driven by input from the ventral hippocampus (vHPC) (Adhikari et al., 2011; Ciocchi et al., 2015; Padilla-Coreano et al., 2016); suppressing this input disrupts these representations and open arm avoidance (Padilla-Coreano et al., 2016). We find that VIP interneurons disinhibit prefrontal responses to vHPC input, suggesting that they may contribute to prefrontal open arm representations and open arm avoidance specifically by enhancing the impact of vHPC inputs on mPFC circuits. Consistent with this model, we find that the effects of VIP interneurons on open arm avoidance change depending on the current strength of vHPC input to mPFC. Together, these results show how the recruitment of prefrontal VIP interneurons at specific times elicits synaptic actions that change network activity in ways that reshape behavior.

RESULTS

VIP interneuron activity increases in the open arms of the EPM.

To efficiently measure VIP interneuron activity during EPM exploration, we used fiber photometry (Cui et al., 2013; Gunaydin et al., 2014) in the widely studied VIP-Cre line (Batista-Brito et al., 2017; Fu et al., 2014; Garcia-Junco-Clemente et al., 2017; Kamigaki and Dan, 2017; Khoshkhoo et al., 2017; Pfeffer et al., 2013; Pi et al., 2013) (Fig. 1A). VIP-Cre mice were injected with adenoassociated-virus (AAV1) encoding Cre-dependent GCaMP6s in mPFC. A fiber for transmitting and collecting excitation and emission wavelengths was implanted above the site of virus injection (Fig. 1B). Two weeks after surgery, mice explored the EPM while we measured VIP-GCaMP signals. VIP-GCaMP signals were higher in the center and open arms than the closed arms (Fig. 1C–D), and closely tracked movement into the center or open arms (Fig. 1E and S1A). Importantly, although VIP interneuron activity can be linked to the speed of locomotion in the open field (Fig. S1B) (Fu et al., 2014), we did not find a relationship between speed and prefrontal VIP GCaMP signals in the EPM (Fig. S1C−D). This may reflect the fact that mice did not run as fast in the EPM as in the open field.

We also used fiber photometry to measure signals from parvalbumin (PV) or somatostatin (SOM) interneurons. Both PV-GCaMP and SOM-GCaMP signals were also higher in the open than closed arms. However, the encoding of EPM location (open vs. closed arms) was significantly stronger for VIP-GCaMP signals, than for PV-GCaMP or SOM-GCaMP signals (Fig. S2).

VIP interneuron activity predicts future open arm avoidance vs. exploration.

Several models could explain our finding that VIP interneuron activity is higher in the center and open arms than closed arms. One is that VIP interneuron activity drives open arm exploration. Alternatively, VIP interneuron activity might represent an anxiety-related signal that promotes open arm avoidance. In the latter model, other signals presumably drive exploration, such that decisions to explore vs. avoid reflect a competition between these pro-exploratory signals and VIP activity-driven avoidance. In this case, exploration would occur when exploratory signals outpace increases in VIP interneuron-driven avoidance signals during approaches to the center or open arms. A final possibility is that VIP activity does not influence or predict choices to explore vs. avoid the open arms, but is simply a readout of EPM location.

First, to test whether VIP activity predicts subsequent exploration vs. avoidance, we identified all runs from a closed arm to the center, then classified each according to whether the mouse subsequently avoided or explored the open arms (closed-center-closed vs. closed-center-open runs). VIP-GCaMP signals in the center chamber were significantly lower for closed-center-open than closed-center-closed runs (Fig. 2A). We also looked further back in time, comparing VIP-GCaMP signals in the closed arm, prior to entry into the center. Again, lower VIP-GCaMP signals predicted subsequent open arm exploration (Fig. 2B).

Inhibiting VIP interneurons reduces open arm avoidance.

The preceding suggests that low vs. high VIP activity as mice approach the center chamber promotes subsequent open arm exploration vs. avoidance, respectively. We used optogenetics to directly test this hypothesized causal relationship. Bilateral fiber optics were implanted into the mPFC of VTP-Cre mice injected with Cre-dependent archaerhodopsin (AAV5-DIO-eArch3.0-eYFP; Arch) or eYFP (AAV5-DIO-eYFP) (Fig. 3A and S3A). We confirmed that Arch reliably inhibited VIP interneurons *in vitro* (Fig. 3B). Because VIP-GCaMP signals specifically increased in the center and open arms, we delivered 532nm light to the mPFC whenever mice were within a "stimulation zone," comprising the center, open arms, and a small portion of the closed arms abutting the center. We then compared behavior during three, 3-minute-long epochs: light OFF, followed by light ON (i.e., light was delivered only in the stimulation zone), and finally light OFF again (Fig. 3C). We quantified light-induced changes in open arm avoidance vs. exploration via three analyses. First, during the light ON epoch, there was a significant increase in relative time spent in the open arms and open arm entries for VIP-Arch mice compared to VIP-eYFP cohorts (Fig. 3D). There was also a corresponding decrease in closed arm entries for VIP-Arch mice (Fig. S3B). Second, the change in time spent in the open arms in the light ON epoch compared to the preceding light OFF epoch was significantly greater for VIP-Arch mice (% change in open arm time: 176 ± 64%) than VIP-eYFP cohorts (32 ± 30%) (Fig. 3E). Third, time spent in the open arms was significantly greater in the light ON epoch than the preceding light OFF epoch for VIP-Arch mice (Fig. 3F) but not for VIP-eYFP controls. Interestingly, in VIP-Arch mice, open arm entries remained elevated during the light OFF epoch following the light ON epoch (Fig. 3D). Inhibiting VIP interneurons did not affect distance travelled in the EPM (Fig. S3C). Also notable is that inhibiting VIP interneurons did not affect open arm exploration when light was delivered continuously throughout a 3-minute epoch (Fig. S3D), rather than triggered by entries into the center or open arms (Fig. S3E−G).

The focus of this study is on how VIP interneurons contribute to a specific behavior (open arm avoidance), rather than on how they contribute to the multifaceted entity of "anxiety" more generally. That being said, optogenetic inhibition of VIP interneurons did attenuate other "anxiety-related" behaviors in the marble-burying and light-dark box tests (Fig. S3H −I).

VIP interneurons disinhibit prefrontal responses to hippocampal input.

Given that VIP interneuron activity increases in the open arms and contributes to open arm avoidance, we decided to explore the relationship between prefrontal VIP interneurons and inputs arriving from the ventral hippocampus (vHPC). vHPC inputs to mPFC differentially encode the open vs. closed arms of the EPM (Ciocchi et al., 2015). Furthermore, mPFC neurons which encode the open vs. closed arms phase-lock to the vHPC theta rhythm suggesting they receive strong input from this source (Adhikari et al., 2011). Indeed, inhibiting vHPC-mPFC projections suppresses single-unit mPFC activity that is specific for the open vs. closed arms, and reduces open arm avoidance (Padilla-Coreano et al., 2016). Based on this, we hypothesized that mPFC VIP interneurons might be recruited by vHPC input and regulate prefrontal responses to that input. To test this, we first confirmed that mPFC VIP interneurons receive direct monosynaptic input from vHPC (Fig. S4A−B). We

recorded from mPFC VIP interneurons while stimulating ChR2 in vHPC terminals, and observed EPSCs in VIP interneurons in the presence of TTX (1 uM) + 4-AP (0.1 mM), which isolates monosynaptic responses (Petreanu et al., 2009).

Next, to test how mPFC VIP interneurons regulate prefrontal responses to vHPC input, we recorded from layer 2/3 pyramidal neurons in acute mPFC slices from VIP-Cre mice injected with two viruses: one to drive Cre-dependent expression of halorhodopsin (VIP-eNpHR) in the mPFC, and a second to express ChR2 in vHPC projection neurons. This enabled us to stimulate ChR2 in vHPC terminals with blue light flashes (5 ms at 10 Hz), with or without concomitant optogenetic inhibition of VIP interneurons (vHPC-ChR2; Fig. 4A). Once again, optogenetic stimulation of vHPC terminals elicited excitatory synaptic responses in VIP interneurons; we also confirmed that simultaneous eNpHR stimulation hyperpolarizes VIP interneurons (Fig. S4C). Spiking of layer 2/3 mPFC neurons in response to vHPC input was reduced when we simultaneously inhibited VIP interneurons (Fig. 4B, left). Repeating these experiments in voltage clamp revealed that inhibiting VIP interneurons significantly increases inhibitory synaptic currents evoked by optogenetic stimulation of vHPC terminals, but has no effect on excitatory currents (Fig. 4C). Thus, VIP interneurons normally disinhibit mPFC responses to vHPC input.

Inhibiting VIP interneurons disrupts prefrontal representations of the open arms.

Given that they disinhibit vHPC-mPFC inputs which transmit information about whether mice are in the open vs. closed arms (Adhikari et al., 2011; Ciocchi et al., 2015), we wondered whether prefrontal VIP interneurons might be necessary for prefrontal representations of the open vs. closed arms. To test this, we had to first identify patterns of prefrontal network activity which encode the open vs. closed arms, then determine how these are altered when we inhibit prefrontal VIP neurons. For this, we employed a dual-color microendoscope (nVoke, Inscopix) for combined GCaMP imaging of mPFC activity and activation of eNpHR in VIP interneurons (Fig. 5A–C). We expressed GCaMP nonspecifically in mPFC neurons using the synapsin promoter; eNpHR expression was restricted to VIP interneurons using a Cre-dependent virus in VIP-Cre mice (Methods). Importantly, cross-activation of inhibitory photocurrents by wavelengths used to excite GCaMP was relatively low (Fig. S5A).

To specifically characterize *network-level* activity patterns, including potential nonlinear interactions between different neurons, we computed the (time-varying) matrix of correlations between signals from different neurons (Fig. S5B). Specifically, for each pair of presumed neurons, we calculated the normalized vector dot product between the time series of GCaMP signals from one neuron and the time series of *derivatives* of the GCaMP signal from the other. We computed correlations between GCaMP signals and derivatives, instead of just between pairs of GCaMP signals, to minimize autocorrelations driven by shared background fluorescence. The rationale for this is that the integral of a signal with its derivative is zero over a closed path (for any signal that is *differentiable* in time). Thus, autocorrelation due to shared background fluorescence, which is proportional to the dot product between the background signal and its derivative, should be approximately zero. To verify that this approach works in practice, we analyzed a surrogate dataset (using the same

parameters we used for our actual analysis). Each surrogate dataset signal was composed of an experimentally measured GCaMP signal, shifted in time by a random amount to make the signals independent from each other. Then we added a common signal (scaled by a random factor between −1 and 1) to each surrogate dataset signal to model shared background fluorescence. Correlations between signals in this surrogate dataset were much larger in magnitude than correlations between signals and their derivatives (Fig. S5C, left). We observed a similar difference for correlation distributions obtained from real data (Fig. S5C, right). Thus, computing correlations between GCaMP signals and their derivatives, as we have done, rather than between the signals themselves, minimizes the magnitude of correlations between signals that are nominally independent but include a component representing shared background fluorescence. As a result, this approach should make it easier to resolve physiologically meaningful correlations. Another rationale for using the derivatives of GCaMP signals to characterize network state, is that these derivatives can be more informative about neuronal firing than the GCaMP signals themselves (Markowitz et al., 2018).

Using this approach, we divided each dataset into 2.5 sec epochs, calculated the correlation matrix (between GCaMP signals and the derivatives of GCaMP signals) during each epoch, and classified each epoch based on whether the mouse was in the closed or open arms (Fig. 5D and S5B). This allowed us to determine whether patterns of prefrontal network activity, i.e., correlation matrices, correlate with EPM behavior. Indeed, every pattern of correlations observed during an open arm epoch was more similar to other patterns of correlations observed during different open arm epochs, than to patterns observed during closed arm epochs (Fig. 5E). Left open arm correlations were also more similar to right open arm correlations than to closed arm correlations (Fig. S5D, top), confirming that these correlations encode anxiety-related (as opposed to purely spatial) information. Importantly, this was not simply due to open arm epochs being close together in time. To show this, we time-shifted all epochs by a fixed amount, persevering their relative timing but shuffling their associated labels (i.e. open vs. closed arms). In time-shifted data, there was no difference between the left-right open arm correlation similarity and the left open arm-closed arm correlation similarity (Fig. S5D, bottom). This finding also validates our analytical approach, because it shows that the correlation matrices we computed carry information about whether the mouse is in the open vs. closed arms.

We then evaluated how inhibiting VIP interneurons affects this encoding of the open vs. closed arms. Strikingly, *differences* in correlations between the open and closed arms were attenuated when we inhibited VIP interneurons (Fig. 5F–G), consistent with the behavioral effect of such inhibition to attenuate the preference for the closed vs. open arms. Importantly, only the magnitude of *changes* in correlations between the open vs. closed arms was altered by inhibiting VIP interneurons; the magnitude of correlations themselves was not different ($p = 1$ by sign-rank test). In fact, when looking on a mouse-by-mouse basis, we found a striking correlation between the degree to which VIP interneuron inhibition attenuates closed vs. open arm differences in correlations, and the degree to which that inhibition attenuates open arm avoidance (Fig. 5H; this analysis controlled for potential sampling bias caused by different amounts of open arm exploration across mice by analyzing the same number of open or closed arm time bins in all mice). Taken together,

these results demonstrate that it is in fact useful to characterize the current state of the prefrontal microcircuit by calculating the matrix of correlations between GCaMP signals and their derivatives, as we have done. Network state, defined in this way, encodes anxiety-related information about whether mice are currently in the open vs. closed arms, and more importantly, predicts the change in open arm exploration that results from inhibiting VIP interneurons.

To delve deeper into this finding, we measured how inhibiting VIP interneurons affected either GCaMP signals or their derivatives in individual neurons. For this, we computed each neuron's "preference index" during the initial light off period and subsequent light on period (Methods). A preference index of 1 or −1 indicates that activity (either GCaMP signals or their derivatives) were consistently higher in the closed or open arms, respectively; 0 indicates that activity was equal in the two chambers. For GCaMP signals, inhibiting VIP interneurons did not significantly alter the distribution of preference indices (Fig. S5E, top). However, for derivatives of GCaMP signals, inhibiting VIP interneurons significantly decreased the absolute value of preferences indices (Fig. S5E, bottom). Thus, inhibiting VIP interneurons disrupts network-level representations of the open vs. closed arms by suppressing the tendency for individual GCaMP signals to preferentially rise in either the open or closed arms.

Inhibiting VIP interneurons only reduces open arm avoidance when hippocampal-prefrontal theta synchrony is strong.

Our previous results show that inhibiting prefrontal VIP interneurons weakens mPFC responses to vHPC input, mPFC representations of the open arms, and open arm avoidance. Based on these observations, we hypothesized that VIP interneurons contribute to open arm avoidance by enhancing the transmission of open arm-related information from vHPC to mPFC. Input from the vHPC to mPFC drives mPFC activity, which differentiates between the open vs. closed arms and open arm avoidance (Adhikari et al., 2011; Ciocchi et al., 2015; Padilla-Coreano et al., 2016). Thus, one model is that inhibiting prefrontal VIP interneurons should only affect open arm avoidance when the vHPC actively transmits information to mPFC, i.e., when vHPC-mPFC communication is strong. An alternative is that prefrontal VIP interneurons make the mPFC more sensitive to weak vHPC input, such that inhibiting prefrontal VIP interneurons selectively impacts open arm avoidance when vHPC-mPFC communication is weak. A third possibility is that prefrontal VIP interneurons regulate open arm avoidance independent of vHPC input to mPFC, i.e., inhibiting VIP interneurons decreases open arm avoidance regardless of whether vHPC-mPFC communication is strong vs. weak. These models are schematized in Fig. 6A.

To distinguish between these models and test whether the role of VIP interneurons in open arm avoidance depends on the current state of the vHPC-mPFC network, we measured vHPC-mPFC theta synchrony during periods of EPM exploration +/− inhibition of VIP interneurons. Theta-frequency synchronization is a marker for communication between vHPC and mPFC, particularly in anxiety-provoking environments such as the EPM (Adhikari et al., 2010; Jacinto et al., 2016; Padilla-Coreano et al., 2016). We implanted stainless steel electrodes within the vHPC and mPFC of VIP-Arch mice (Fig. 6B and S6A).

In the mPFC, the implanted electrode was attached to one side of a bilateral fiber optic implant to record while stimulating Arch in VIP interneurons using the same location-based method described earlier. First, we tested whether inhibiting VIP interneurons directly alters vHPC-mPFC theta synchrony. For this we separated runs which entered the stimulation zone based on whether they exhibited dips or peaks in vHPC-mPFC theta synchrony at specific timepoints. Specifically, at each timepoint we z-scored vHPC-mPFC theta synchrony relative to the rest of the run. Then we separated runs based on whether this z-scored vHPC-mPFC theta synchrony was in the first (bottom), second, third, or fourth (top) quartile (Supplementary Table 1; Fig. 6C and S6B). The distribution of runs in each quartile did not differ between the light ON vs. OFF conditions at the time of stim-zone entry (t = 0) or during the next 1.5 seconds (chi-squared test, $p = 0.34$ and 0.35, respectively). This indicates that real-time inhibition of VIP interneurons does not trigger immediate changes in theta synchrony.

Next, we examined whether inhibiting VIP interneurons increases open arm exploration under all conditions, or only when vHPC-mPFC communication is strong or weak, i.e., when the z-scored theta synchrony is in the top or bottom quartile, respectively. For this we plotted the fraction of runs which avoid vs. explore the open arms as a function of quartile and light ON vs. OFF. When we inhibited VIP interneurons (light ON), we observed a dramatic increase in the fraction of *top quartile* runs (relatively high theta synchrony) that explored the open arms (Fig. 6D). In fact, the majority of such runs now explored the open arms. By contrast, there was no significant change in the fraction of runs in the *bottom quartile* – those associated with dips in theta synchrony – which explored the open arms (Fig. 6C). We also did not see a significant change in open arm runs for the second or third quartiles of theta synchrony (Fig. S6B). Thus, inhibiting VIP interneurons only increases open arm exploration when vHPC-mPFC theta synchrony increases, which presumably reflects the transmission of anxiety-related information from vHPC to mPFC. By contrast, when theta synchrony dips (and vHPC-mPFC input is presumably not contributing to open arm avoidance), inhibiting VIP interneurons has no effect on open arm exploration.

As a control, we also identified runs based on the top quartile of delta (1–4 Hz), beta (13–30 Hz), or gamma (low: 30–58 Hz; high: 62–120 Hz) synchrony. In these cases, light delivery did not significantly alter the relative number of open vs. closed arm runs (Fig. S6C).

DISCUSSION

We have elucidated the role of prefrontal VIP interneurons in a distributed hippocampal-prefrontal network regulating open arm avoidance in the EPM. Prefrontal VIP interneurons not only encode whether mice are in the open/closed arms of the EPM, but more strikingly, predict future open arm exploration vs. avoidance. VIP interneurons receive vHPC input and disinhibit prefrontal responses to that input. Inhibiting VIP neurons disrupts the prefrontal encoding of open vs. closed arms. This specifically increases open arm exploration during periods of high vHPC-mPFC theta synchrony, which indicate the transmission of anxiety signals from vHPC to mPFC. These observations suggest that prefrontal VIP interneurons normally disinhibit prefrontal responses to vHPC input, thereby helping to generate prefrontal representations of the open vs. closed arms, which contribute to open arm

avoidance. Specifically high VIP interneurons activity in the open arms will enhance prefrontal responses to vHPC inputs during open arm exploration, producing patterns of open arm activity distinct from those observed in the closed arms, as seen in our imaging experiments. This is schematized in Fig. 6E.

These results show that VIP interneurons are recruited by, and powerfully modulate, a behavior widely studied because of its presumed relevance to anxiety. In particular, our findings that VIP activity in the EPM does not correlate with running speed, but that VIP activity in a single location (the closed arm) differs based on future behavior (whether mice explore vs. avoid the open arms when they subsequently enter the center), suggests that VIP interneurons encode behavioral state, not just sensorimotor signals. Our findings also show that VIP interneurons disinhibit cortical responses to a particular source of input, are necessary for network-level representations known to depend on that input, and elicit behavioral effects that correlate strongly with changes in these network-level representations. Together, these data connect the actions of VIP interneurons across the cellular, synaptic, microcircuit, and distributed network levels, revealing the details of a mechanism through which they can alter a specific behavior.

There are multiple possible reasons why inhibiting VIP interneurons might decrease open arm avoidance. This manipulation might make mice unable to differentiate the open vs. closed arms, reduce physiological measures of anxiety (e.g., elevated heart rate), or simply cause mice to ignore those anxiety signals as they make decisions about whether to explore vs. avoid. Notably, inhibiting VIP interneurons while mice are exploring the EPM causes an increase in open arm exploration which outlasts the period of inhibition (Fig. 3D). If inhibiting VIP interneurons simply renders mice unaware of whether they are in the open or closed arms, then it is hard to imagine why this would lead to long-lasting changes in open arm avoidance. Future experiments could address whether inhibiting VIP interneurons reduces physiological measures of anxiety or causes mice to ignore those signals by measuring the effects of inhibiting VIP interneurons on variables such as heart rate. In addition, most of our behavioral experiments (Fig. 1–3) used male mice only. Other behavioral experiments (Fig. 5–6) used male and female mice, but in these cases, group sizes were too small to examine possible sex differences. These could be evaluated by future experiments.

Location-based, but not continuous, inhibition of VIP interneurons disrupts open arm avoidance

Inhibiting VIP interneurons disrupts open arm avoidance when inhibition is delivered selectively within a stimulation zone, but not when delivered continuously throughout a 3-minute epoch. There are many possible explanations for this. First, EPM behavior may be particularly sensitive to changes in avoidance signals, i.e., decisions about whether to explore vs. avoid may depend on the rate at which avoidance signals rise as mice enter the center zone. In this scenario, triggering inhibition as mice approach the center may be especially effective at blunting rises in VIP interneuron activity which normally promote avoidance. Alternatively, continuous inhibition may elicit circuit adaptations which reduce

its effectiveness. Interestingly, continuous eNpHR stimulation throughout a 3-minute epoch does appear to effectively suppress spiking in individual VIP interneurons (Fig. S3D).

Inhibiting VIP interneurons only disrupts open arm avoidance when vHPC-mPFC theta synchrony is high.

The behavioral effects of inhibiting VIP interneurons depended strongly on the level of vHPC-mPFC theta synchrony. When synchrony was relatively high, inhibiting VIP interneurons increased open arm exploration by ~600%. By contrast, when synchrony was relatively low, inhibiting VIP interneurons did not alter open arm exploration. This is consistent with a model in which VIP interneurons normally contribute to open arm avoidance specifically by enhancing the transmission of strong anxiety-related signals from hippocampus to prefrontal cortex. Theta synchrony is thought to be a biomarker for anxiety-related communication between these structures (Adhikari et al., 2010; Jacinto et al., 2016; Padilla-Coreano et al., 2016). Thus, when theta synchrony is high, a channel for anxiety-related communication between the vHPC and mPFC is effectively "open." Under these conditions, VIP interneurons can enhance prefrontal responses to the anxiety-related input coming from vHPC, thereby promoting open arm avoidance. By contrast, when theta synchrony is low, vHPC input to mPFC is either weak or unrelated to anxiety; under these conditions, the anxiety-related channel from vHPC to mPFC is effectively "closed." As a result, VIP interneurons do not contribute to open arm avoidance, and inhibiting them does not affect EPM behavior. This demonstrates that VIP interneurons do not exert a *network-autonomous* effect on prefrontal circuits, i.e., VIP interneurons do not simply enhance the output of specific set of prefrontal neurons that drive open arm avoidance. VIP interneurons also do not seem to amplify the behavioral effects of weak vHPC input – if they did, then the effects of inhibiting VIP interneurons should have been greatest when vHPC-mPFC theta synchrony is relatively low. Rather, the behavioral effects of inhibiting VIP interneurons are determined by the state of vHPC-mPFC communication, and VIP interneurons seem to specifically enhance the ability of strong hippocampal input to generate avoidance signals in prefrontal circuits.

Interestingly, we found that mice avoid the open arms, even when vHPC-mPFC theta synchrony is low (Fig. 6D). Under these conditions, open arm avoidance may be driven by signals which do not depend on vHPC-mPFC communication or mPFC VIP interneurons. Alternatively, when vHPC-mPFC theta synchrony is low, both exploratory and avoidance signals may be weak. As a result, inhibiting prefrontal VIP interneurons might fail to reduce open arm avoidance when vHPC-mPFC theta synchrony is low, because exploratory signals needed to drive open arm entries are absent.

Finally, the prelimbic (PL) and infralimbic (IL) divisions of the mPFC play different roles in fear conditioning and extinction (Do-Monte et al., 2015; Sierra-Mercado et al., 2011). By contrast, studies that have used the EPM have generally not distinguished between these subregions nor described distinct functions of PL vs. IL in EPM behavior (Adhikari et al., 2010; Adhikari et al., 2011; Ciocchi et al., 2015; Jacinto et al., 2016; Kjaerby et al., 2016; Padilla-Coreano et al., 2016). We consistently implanted fiber optics near the PL/IL border

and thus did not explore potential differences between the roles of PL and IL in EPM behavior, which could be addressed by future studies.

Conclusions

Previous studies of VIP interneurons have emphasized their role in disinhibition and increasing signal-to-noise at the single neuron level (Ayzenshtat et al., 2016; Fu et al., 2014; Kamigaki and Dan, 2017; Karnani et al., 2016; Lee et al., 2013; Pi et al., 2013). These single neuron changes can affect network representations (Ayzenshtat et al., 2016; Kamigaki and Dan, 2017). Here, we reveal two additional features about how VIP interneurons act at the network level to influence behavior (Fig. 6E). First, the degree to which manipulating VIP interneuron activity disrupts network-level representations of behaviorally-relevant information, predicts the extent to which behavior changes as a result of this manipulation ($R^2 \sim 0.9$). This is a key piece of evidence that the specific changes in network activity we identified may link changes in VIP interneuron activity with changes in behavior – at the very least, these patterns of network activity represent a highly informative biomarker for changes in behavior. Second, the behavioral effects of inhibiting VIP interneurons depend critically on the current state of the network. This shows that VIP interneurons do not simply excite or inhibit cells which drive open arm avoidance. Rather, VIP interneurons enable cortical circuits to integrate specific sources of input into emergent network-level representations that guide complex behaviors.

STAR METHODS

Further information and requests for resources and reagents should be directed to and will be fulfilled by the Lead Contact, Vikaas Sohal (vikaas.sohal@ucsf.edu).

All experiments were conducted in accordance with procedures established by the Administrative Panels on Laboratory Animal Care at the University of California, San Francisco.

Experimental Model and Subject Details

The following mouse lines (> 4 wks old) were used for behavior or photometry experiments: Vip<tm1(cre)Zjh>/J (line 010908; www.jax.org), Sst<tm2.1(cre)Zjh>/J (line 013044; www.jax.org), and B6;129P2-Pvalb<tm1(cre)Arbr>/J (line 008069; www.jax.org). Experiments using fiber photometry or optogenetic inhibition only were done with male mice only. For experiments which combined optogenetic inhibition + microendoscopic GCaMP imaging (n = 6 mice) or optogenetic inhibition + multisite LFP recording (n = 4 mice), we used both male and female mice but did not analyze the effects of sex due to the limited group size, which precluded population-level analyses in these experiments.

Virus injection and fiber implantation for photometry and optogenetic experiments

After isofluorane anesthesia, the scalp and periosteum were removed from the dorsal surface of the skull and scored with a scalpel to improve implant adhesion. For animals used in photometry experiments, 4 × 0.150ul of AAV2/1-Syn-FLEX-GCaMP6s (Penn Vector Core) was injected unilaterally at 4 depths (DV: −2.0, −2.25, −2.5, −2.75) at the following AP/ML

(millimeters We waited 2–3 weeks before beginning behavioral experiments. For optogenetic experiments, 0.750 μl of AAV5-EF1 a-DIO-eArch3.0-eYFP or AAV5-EF1 a-DIO-eYFP (UNC Vector Core) was injected bilaterally into the medial PFC (mPFC) (Sohal et al., 2009). Coordinates for injection into mPFC were 1.7 (AP), 0.3 (ML), and −2.6 dorsoventral (DV). We waited at least 4 weeks after injection before behavioral experiments to allow for viral expression. Mice from a single litter were arbitrarily assigned to different experimental groups.

Surgical methods for fiber photometry implantation were based from protocols from Gunaydin et al., 2014. After injection of GCaMP virus, a 400/430 μm (core/outer) diameter 0.48-NA multimode fiber implant (Doric Lenses: #400/430–0.48) was slowly inserted into the mPFC until the tip of the fiber reached a DV depth of −2.25. For optogenetic behavior experiments, 200/240 μm 0.22NA dual-fiber cannulas were inserted into the mPFC at a DV depth of −2.25. Implants were affixed onto the skull using Metabond dental cement (Parkell).

Fiber photometry design and analysis

The photometry apparatus was based on the design described by Gunaydin et al., 2014. A 100mW Omicron 470mW laser was optically chopped (Thorlabs, MC2000) and cleaned-up by a 470/20nm filter (Thorlabs) before hitting a 495 nm dichroic mirror (Semrock) and focused onto a custom-made 0.48-NA, 400μm multimode patch cable (Thorlabs, BFH48–400) via a FC/PC fiber collimator (Thorlabs, F240FC-A). The patch cable was friction-fit via a ferrule sleeve (Thorlabs) onto an optical fiber (Doric Lenses, #400/430–0.48) implanted into the brain as described above. A 530/20nm lens (Thorlabs) filtered the emitted light before being detected by a femtowatt photoreceiver (Newport, Model 2151). The photoreceiver was attached to a X-Y translator (Thorlabs, ST1XY-A) and adjustable lens tube (Thorlabs, SM1NR1) to assist in aligning the light path. Emitted light was focused onto the photoreceiver via a plano-convex lens (Thorlabs, F = 50.0, N-BK7) housed in the lens tube. All optical equipment were mounted onto an aluminum breadboard (Thorlabs). A lock-in amplifier (Stanford Research Systems, SR810 DSP) whose sampling interval was locked to the optical chopper filtered the signals from the photoreceiver. A digital acquisition board (Labjack) streamed the data onto a personal computer for off-line data analysis.

For calculating mean GCaMP signals during eventual open vs. closed arm runs, an observer scored each run (as an eventual open vs. closed arm run) and marked the frames where the animal initiated its run, entered/exited the center zone, and ended its run. The observer was blinded to the corresponding GCaMP signals during this analysis.

Behavioral assays

Mice were housed in reversed 12-h light/dark cycles, and all experiments were performed during the dark portion of the cycle. After sufficient time for surgical recovery and viral expression, mice underwent multiple rounds of habituation. The testing room was illuminated at 150 lux, and mice were first habituated to the behavioral testing area for 30 minutes prior to the beginning of any further handling each day. Mice were then habituated to touch with at least 3 days of handling for ~5 min each day, followed by 1–2 days of

habituation to the optical tether in their home cage for 10 min. Next, mice were placed into a larger housing cage for 1–2 days for 10 min where they habituated to the tether as they explored the novel environment.

Elevated plus maze: After habituation, behavior was assessed using the elevated plus maze (EPM). EPM sessions lasted 9 minutes, with the laser stimulation delivered during the second three-minute epoch to activate Arch (532nm, 6–8mW total). eYFP-expressing mice served as controls, i.e., they also received continuous 532nm light when in the stimulation zone. Real-time light delivery was based on the location in the EPM apparatus, with the stimulation zones demarcated as the open arms, center zone, and the closed arm zone proximal (within one quarter-length) to the center zone.

Marble burying test: The marble-burying assay was performed as described in (Kedia and Chattarji, 2014). Mice were allowed to explore a standard mouse cage filled with white Alfa Dry bedding (depth of 4–5 cm) for 10 minutes for habituation. Twenty glass marbles were then placed in a 4×5 configuration, and mice were allowed to explore the cage for another 20 minutes, during which we performed video recording for subsequent offline analysis. Optogenetic stimulation (continuous 532nm light, ~5–7mW) was delivered in alternating 5 min-long epochs (light ON, light OFF, light ON, light OFF). An experimenter, blinded to the virus injected into each mouse (eYFP vs. eArch), scored the video recordings to determine the 1) latency to dig during epoch one, and 2) total time spent digging during light ON epochs. One mouse was excluded from analysis due to its optical tether being caught by the lixit port.

Light-dark box test: The light-dark box was designed as described in (Anthony et al., 2014) with the following dimensions (overall, 50 × 25 × 30 cm): light side 31 cm long, dark side 16 cm long; doorway between light and dark sides, 5.25 cm wide and 3 cm long. Mice were placed into the dark side of the chamber, and the optogenetic stimulation was triggered by entry into the center tunnel and light side of the box during the light ON epochs. The entire experiment consisted of 4 minute-long epochs in the following order: light OFF, light ON, light OFF.

A USB webcam (Logitech) connected to a computer running ANY-maze (Stoelting) was used to track the position of the mouse in behavioral apparatuses, trigger optogenetic stimulation, and sync electrophysiology data to animal position. Analyses were performed offline using custom MATLAB code. The sample sizes of our cohorts are in ranges commonly found in experiments using elevated plus maze to assay anxiety-like behaviors. Animals were randomly assigned to a virus cohort (eArch vs eYFP), and the experimenter was blinded to each mouse's virus assignment when the behavioral assessment was performed.

Slice preparation and in vitro recording parameters

Slice preparation and intracellular recording followed our published protocol (Sohal and Huguenard, 2005). Briefly, we cut 250 μm coronal slices from 8- to 11-week-old mice of either sex and secured the tissue onto the recording platform using a harp. Whole-cell patch

recordings were obtained from VIP cells expressing fluorophore-labeled opsins or visually identified pyramidal cells in layer II/III of infralimbic or prelimbic cortex using differential contrast video microscopy on an upright microscope (BX51WI; Olympus). Recordings were made using a Multiclamp 700A (Molecular Devices). For voltage-clamp recordings, patch electrodes (tip resistance = 2–6 MΩ) were filled with the following (in mM): 130 Cs-methanesulfonate, 4 NaCl, 2 $MgCl_2$, 10 EGTA, 10 HEPES, 5 TEA, 5 QX-314, 2 MgATP, and 0.5 Na_3GTP (pH adjusted to 7.2 with CsOH). Cells were held at −70 mV and +10 mV to isolate EPSCs and IPSCs, respectively (Fig. 4C). For recordings of cell-intrinsic properties, patch electrodes (tip resistance = 1–4 MOhms) were filled with the following (in mM): 130 K-gluconate, 10 KCl, 10 HEPES, 10 EGTA, 2 MgCl, 2 MgATP, and 0.3 NaGTP (pH adjusted to 7.3 with KOH). All recordings were at 32.0±1°C. Series resistance was usually 10–20 MQ, and experiments were discontinued above 25 MΩ.

The Vip<tm1(cre)Zjh>/J (line 010908; www.jax.org) mouse line was used for slice experiments.

A light-emitting LED engine (Lumencor) was used to elicit photo-induced currents. We stimulated ChR2-infected fibers or cell bodies with ~1–3 mW of 470 nm light with pulses of 5 ms in duration. eArch-infected cell bodies were stimulated with ~4–5 mW of 550/15 nm light. The light path was delivered to the slice via a 40x objective (Olympus) and illuminated across the full high-power (40x) field.

For patch-clamp experiments measuring the effects of VIP interneuron inhibition on responses to theta frequency stimulation of vHPC inputs, VIP-ires cre mice were injected with 2× 0.450ul of AAV5-EF1 a-DIO-eNpHR3.0-mCh (“eNpHR”; DV: −2.3, −2.6; UNC Vector Core) using the stereotactic coordinates for mPFC listed earlier, and 0.650ul of AAV5-CaMKII-ChR2-eYFP (UNC Vector Core) into the vHPC (−3.25 AP, 3.1 ML, −4.1 DV). Coronal slices were prepared ~5 weeks later, and ChR2 expression in the ventral hippocampus was confirmed in all cases at the start of each experiment. To increase the spontaneous network activity in vitro, active aCSF (3.5mM KCl, 11mM glucose, 123mM NaCl, 1.25 NaH_2PO_4, 1mM $MgCl_2$, 1mM $CaCl_2$, 1mM $MgSO_4$) was washed on for five minutes after initiating each recording from a layer 2/3 pyramidal neuron. We targeted visually-identified layer 2/3 pyramidal neurons adjacent to eNpHR-infected VIP neurons for recording (Fig. 4A). The optogenetic stimulation protocol comprised of 80sec long sweeps. Each sweep was broken up as follows: a 10 sec period of ChR2 stimulation (1–5mW, 5ms light flashes delivered at 10 or 25Hz using a LED engine (Lumencor) emitting 440/20 nm and 470/24nm), followed by a 30sec recovery period, then another 10 sec period of concurrent ChR2 + eNpHR stimulation (constant 2mW light, with the LED engine emitting 640/30nm). DC current (20–60pA) was injected to elicit submaximal levels of spiking. Cells with unstable resting membrane potentials were excluded from analyses.

For patch-clamp experiments verifying levels of cross-activation by GCaMP excitation wavelength on halorhodopsin photocurrents, VIP-ires-cre mice were injected with 2× 0.450ul of AAV5-EF1a-DI0-eNpHR3.0-mCh (DV: −2.3, −2.6; UNC Virus Core) using mPFC stereotactic coordinates described earlier, and coronal sections were harvested ~5 weeks later. We then patched clamped prefrontal VIP neurons infected with Cre-dependent

halorhodopsin while administering light approximating in vivo recording conditions: GCaMP excitation light (470nm, 200uW) and halorhodopsin excitation light (640/30nm, 2.25mW). Our LED engine was unable to deliver greater than 2.25mW of 600nm light in vitro.

Surgery and analysis of LFP experiments

Following virus injection, standard-tip 0.5 MΩ-impedance stainless steel electrodes (Microprobes, SS30030.5A10) were inserted into the mPFC, vHPC, and BLA. For the mPFC location, an optrode (optical fiber + electrode) was custom-made by affixing the electrode to the right optical fiber of a dual-fiber cannula. The tip of the electrode protruded beyond the fiber tip by 200–500μm. The coordinates for vHPC and BLA were as follows: vHPC, −3.25 (AP), 3.1(ML), −4.1 (DV); BLA, −1.34 (AP), 3.12 (ML), −4.74 (DV). A common reference screw was implanted into the cerebellum (500 μm posterior to lambda) and a silver ground wire was placed underneath the left lateral scalp. After affixing the electrodes in place using Metabond, connections were made to the headstage of a multi-channel recording system (Pinnacle). All channels shared a common reference (cerebellum). Data was collected at 2000 Hz and band-pass filtered 1–200Hz at the pre-amp. Electrode placement was verified histologically. We also examined the power spectra from all electrodes; only animals with vHPC power spectra that exhibited a visible peak in the theta frequency range were used for further analysis. (Note for one mouse, we were not able to verify the localization of the vHPC electrode because the brain was blocked too far rostrally during histology; however, we did not exclude this mouse from analysis because its vHPC electrode exhibited a clear theta peak).

Analysis of LFP data was facilitated using custom MATLAB code. The LFP signals were FIR-filtered (filter length 3x period corresponding to minimum frequency of frequency band) and Hilbert transformed to yield the instantaneous amplitudes (magnitude) and phases (angle). The amplitude covariation between regions in a particular frequency band was calculated by the maximum normalized cross correlation of the instantaneous band-pass filtered amplitudes of each electrode. Amplitude covariation in the theta, beta, and gamma bands was calculated using a 2.5 second window, at 1.5 sec intervals from 7.5 seconds before to 7.5 seconds after the animal entered the stimulation zone of the EPM. For the delta band, amplitude covariation was calculated using a 10 second window (in order to sample a similar number of cycles). Amplitude covariation was individually z-scored for each stim-zone entry, i.e., each run. Each run is an approach to the center starting from a closed arm. A run was defined as an open run if mice proceeded into the open arms and closed run if they either crossed through the center directly to the other closed arm or retreated back into the starting arm. Z-scored amplitude covariation values were classified into quartiles by pooling z-scores from all mice and all conditions.

Surgery, histology, and analysis of optogenetic endoscope experiments

For endoscope experiments, 4× 0.150ul of AAV1-Syn-GCaMP6m (DV: −2.0, −2.25, −2.5, −2.75; diluted 1:4; UPenn Virus Core) and 2× 0.450ul of AAV5-EF1 a-DIO-eNpHR3.0-mCh (DV: −2.3, −2.6; UNC Virus Core) were injected into the mPFC using stereotactic coordinates described earlier. Following viral injection, a 0.5mm diameter x 6.1mm long

GRIN lens (Inscopix) was slowly advanced into the mPFC until the tip was placed at DV −2.25 and cemented in place with Metabond dental cement. After 2–3 weeks of viral expression, an imaging baseplate was positioned over the GRIN lens and cemented in place. The mice were allowed to recover for another 2 weeks before the beginning of habituation.

Mice were perfused using standard transcardial perfusion with PBS and 4% PFA, and brains were post-fixed for at least one day. Tissue (75 μm thick coronal sections) was obtained on vibratome, and immunohistochemistry was performed on floating 75 μm coronal sections using chicken anti-GFP (1:1000, Aves Lab, GFP-1020), rabbit anti-DsRed (1:500; Clontech, #632496) antibodies, and corresponding AlexaFluor 488 and 594 secondary goat antibodies (1:500; Invitrogen, A-11039, R37117). Images were obtained on a Zeiss LSM confocal.

nVistaHD and nVoke software (Inscopix) were used to control the microscope and collect imaging data. Images were acquired at 20 frames per second using an imaging LED power of ~150–250 μW and stored off-line for data processing. An input TTL from a separate Anymaze computer triggered the optogenetic LED (6–8 mW) and synced imaging timestamps to positional tracking.

Imaging data was downsampled 2x in the x- and y- directions. To increase contrast for motion correction, frames were FFT bandpass filtered (3–40 pixels; ImageJ) and an unsharp mask (radius 10 pixels, 0.60 mask weight; ImageJ) was applied. Motion correction was then performed using a template-matching algorithm (normalized correlation coefficient; ImageJ) with a high-contrast subregion selected as the reference. Analysis of the dataset using a modified PCA/ICA approach (Luongo et al., 2016a; Luongo et al., 2016b) detected 80–90 ROIs (presumed neurons) per field of view (Fig. 5B).

To describe patterns of local microcircuit activity, matrices of correlations between VIP signals and their time derivatives were calculated with a window of 2.5 sec and matched to the mouse's EPM position (in closed vs open arm). Specifically, we calculated each correlation by computing the normalized vector dot product between a time series of GCaMP signals and a time series of derivatives (corresponding to a different neuron). The example closed and open arm correlation matrices in Fig. 5D were generated by finding the mean of twenty randomly selected correlation matrices from in-closed and in-open arm periods for one mouse. To calculate the similarity of open arm correlation matrices to other open or closed arm correlation matrices in Fig. 5E, we calculated the matrix dot-product of an individual open arm correlation matrix with every other open or closed arm matrix and plotted the mean matrix dot-product for open (x-axis) and closed (y-axis) arm comparisons. Thus, each point in Fig. 5E marks the average similarity of a given open arm correlation matrix to all other closed (y-axis) or open (x-axis) arms. Likewise, each open arm epoch was assigned either a left or right open arm position, and the similarity was computed for each left open arm correlation matrix with every right open (x-axis) or closed arm (y-axis) matrix in Fig. S4C. Fig. 5F describes how the distribution of correlations with significant ($p < 0.01$) differences between closed and open arm is altered by VIP inhibition. First, open and closed arm correlation matrices were collected for each three-minute epoch. For each neuron, an unpaired student's t-test was used to determine if that given neuron had correlations that were statistically significant ($p < 0.01$) between closed and open arms. To determine the

change in correlation between open and closed arms, the mean correlation of closed arms was subtracted from the mean correlation of open arms for each neuron. Thus, each panel in Fig. 5F shows the distribution of correlations that significantly increased or decreased between closed and open arms in epoch one (top) and two (bottom) with a significance set at $p < 0.01$. To correlate the effect of VIP inhibition on distribution of significantly different correlations (Fig. 5G–H), we determined the percent-change, from epoch 1 to 2, in correlation strength, which was simply the distance between means (Fig. 5F, red arrows).

Calculation of preference index values

The preference index (P.I.) value of each cell was calculated by first assigning pixel values to a map of the EPM based on the cumulative sum of the z-scored calcium signal or its time-derivative whenever the mouse is physically occupying a pixel on the EPM map. This cumulative map is then normalized by the amount of time the mouse spends in each pixel on the EPM map. The top 5% of pixels of the normalized map are then considered significant pixels, and P.I. is calculated by:

$$P.I. = \frac{P_o - P_c}{P_o + P_c}$$

where P_o is the percentage of significant open-arm pixels and P_c is the percentage of significant closed-arm pixels, over all open- and closed-arm pixels respectively. The open-arm pixels are defined as the areas comprising the open arms and the center of the EPM, while the closed-arm pixels make up the rest of the EPM. This procedure can be repeated separately for each of the three epochs to get the P.I. for each cell during each of the three epochs.

Statistics, data analysis, and data availability

Unless otherwise specificed, nonparametric tests or ANOVA was used to assess signficance. Statistics were calculated using either custom MATLAB code or Graphpad Prism. All statistical parameters, including test statistics, correction for multiple comparisons, and sampling of repeated measurements are stated in the main text. All tests are two-sided, and error bars represent SEM. The code and data used to generate and support the findings of this study are available from the corresponding author upon reasonable request.

Supplementary Material

Refer to Web version on PubMed Central for supplementary material.

ACKNOWLEDGEMENTS

Alice Stamatakis, Stephanie Otte, and Inscopix Inc. provided the nVoke system and technical support. AL, MC, FL, IE, SP, and VS are supported by NIH/OD (DP2 MH100011), NIMH (R01 MH100292), the BRAIN initiative (U01 MH105948), the Simons Foundation (399853), and a Weill Institute for Neurosciences Trailblazer award. AL is additionally supported by NIMH (F30 MH106272), a J. Michael Bishop Fellowship, and NIGMS (Medical Scientist Training Program Grant GM07618). IE is supported by NIMH (K01 MH097841).

REFERENCES

Adhikari A, Topiwala MA, and Gordon JA (2010). Synchronized activity between the ventral hippocampus and the medial prefrontal cortex during anxiety. Neuron 65, 257–269. [PubMed: 20152131]

Adhikari A, Topiwala MA, and Gordon JA (2011). Single units in the medial prefrontal cortex with anxiety-related firing patterns are preferentially influenced by ventral hippocampal activity. Neuron 71, 898–910. [PubMed: 21903082]

Anthony TE, Dee N, Bernard A, Lerchner W, Heintz N, and Anderson DJ (2014). Control of stress-induced persistent anxiety by an extra-amygdala septohypothalamic circuit. Cell 156, 522–536. [PubMed: 24485458]

Ayzenshtat I, Karnani MM, Jackson J, and Yuste R. (2016). Cortical Control of Spatial Resolution by VIP+ Interneurons. J Neurosci 36, 11498–11509. [PubMed: 27911754]

Batista-Brito R, Vinck M, Ferguson KA, Chang JT, Laubender D, Lur G, Mossner JM, Hernandez VG, Ramakrishnan C, Deisseroth K, et al. (2017). Developmental Dysfunction of VIP Interneurons Impairs Cortical Circuits. Neuron 95, 884–895 e889. [PubMed: 28817803]

Ciocchi S, Passecker J, Malagon-Vina H, Mikus N, and Klausberger T. (2015). Brain computation. Selective information routing by ventral hippocampal CA1 projection neurons. Science 348, 560–563. [PubMed: 25931556]

Cui G, Jun SB, Jin X, Pham MD, Vogel SS, Lovinger DM, and Costa RM (2013). Concurrent activation of striatal direct and indirect pathways during action initiation. Nature 494, 238–242. [PubMed: 23354054]

Do-Monte FH, Manzano-Nieves G, Quinones-Laracuente K, Ramos-Medina L, and Quirk GJ (2015). Revisiting the role of infralimbic cortex in fear extinction with optogenetics. J Neurosci 35, 3607–3615. [PubMed: 25716859]

Fu Y, Tucciarone JM, Espinosa JS, Sheng N, Darcy DP, Nicoll RA, Huang ZJ, and Stryker MP (2014). A cortical circuit for gain control by behavioral state. Cell 156, 1139–1152. [PubMed: 24630718]

Garcia-Junco-Clemente P, Ikrar T, Tring E, Xu X, Ringach DL, and Trachtenberg JT (2017). An inhibitory pull-push circuit in frontal cortex. Nat Neurosci 20, 389–392. [PubMed: 28114295]

Gunaydin LA, Grosenick L, Finkelstein JC, Kauvar IV, Fenno LE, Adhikari A, Lammel S, Mirzabekov JJ, Airan RD, Zalocusky KA, et al. (2014). Natural neural projection dynamics underlying social behavior. Cell 157, 1535–1551. [PubMed: 24949967]

Jacinto LR, Cerqueira JJ, and Sousa N. (2016). Patterns of Theta Activity in Limbic Anxiety Circuit Preceding Exploratory Behavior in Approach-Avoidance Conflict. Front Behav Neurosci 10, 171. [PubMed: 27713693]

Kamigaki T, and Dan Y. (2017). Delay activity of specific prefrontal interneuron subtypes modulates memory-guided behavior. Nat Neurosci 20, 854–863. [PubMed: 28436982]

Karnani MM, Jackson J, Ayzenshtat I, Hamzehei Sichani A, Manoocheri K, Kim S, and Yuste R. (2016). Opening Holes in the Blanket of Inhibition: Localized Lateral Disinhibition by VIP Interneurons. J Neurosci 36, 3471–3480. [PubMed: 27013676]

Kedia S, and Chattarji S. (2014). Marble burying as a test of the delayed anxiogenic effects of acute immobilisation stress in mice. J Neurosci Methods 233, 150–154. [PubMed: 24932962]

Khoshkhoo S, Vogt D, and Sohal VS (2017). Dynamic, Cell-Type-Specific Roles for GABAergic Interneurons in a Mouse Model of Optogenetically Inducible Seizures. Neuron 93, 291–298. [PubMed: 28041880]

Kjaerby C, Athilingam J, Robinson SE, Iafrati J, and Sohal VS (2016). Serotonin 1B Receptors Regulate Prefrontal Function by Gating Callosal and Hippocampal Inputs. Cell Rep 17, 2882–2890. [PubMed: 27974203]

Lee S, Kruglikov I, Huang ZJ, Fishell G, and Rudy B. (2013). A disinhibitory circuit mediates motor integration in the somatosensory cortex. Nat Neurosci 16, 1662–1670. [PubMed: 24097044]

Luongo FJ, Horn ME, and Sohal VS (2016a). Putative Microcircuit-Level Substrates for Attention Are Disrupted in Mouse Models of Autism. Biol Psychiatry 79, 667–675. [PubMed: 26022075]

Luongo FJ, Zimmerman CA, Horn ME, and Sohal VS (2016b). Correlations between prefrontal neurons form a small-world network that optimizes the generation of multineuron sequences of activity. J Neurophysiol 115, 2359–2375. [PubMed: 26888108]

Markowitz JE, Gillis WF, Beron CC, Neufeld SQ, Robertson K, Bhagat ND, Peterson RE, Peterson E, Hyun M, Linderman SW, et al. (2018). The Striatum Organizes 3D Behavior via Moment-to-Moment Action Selection. Cell 174, 44–58 e17. [PubMed: 29779950]

Padilla-Coreano N, Bolkan SS, Pierce GM, Blackman DR, Hardin WD, Garcia-Garcia AL, Spellman TJ, and Gordon JA (2016). Direct Ventral Hippocampal-Prefrontal Input Is Required for Anxiety-Related Neural Activity and Behavior. Neuron 89, 857–866. [PubMed: 26853301]

Petreanu L, Mao T, Sternson SM, and Svoboda K. (2009). The subcellular organization of neocortical excitatory connections. Nature 457, 1142–1145. [PubMed: 19151697]

Pfeffer CK, Xue M, He M, Huang ZJ, and Scanziani M. (2013). Inhibition of inhibition in visual cortex: the logic of connections between molecularly distinct interneurons. Nat Neurosci 16, 1068–1076. [PubMed: 23817549]

Pi HJ, Hangya B, Kvitsiani D, Sanders JI, Huang ZJ, and Kepecs A. (2013). Cortical interneurons that specialize in disinhibitory control. Nature 503, 521–524. [PubMed: 24097352]

Sierra-Mercado D, Padilla-Coreano N, and Quirk GJ (2011). Dissociable roles of prelimbic and infralimbic cortices, ventral hippocampus, and basolateral amygdala in the expression and extinction of conditioned fear. Neuropsychopharmacology 36, 529–538. [PubMed: 20962768]

Sohal VS, and Huguenard JR (2005). Inhibitory coupling specifically generates emergent gamma oscillations in diverse cell types. Proc Natl Acad Sci U S A 102, 18638–18643. [PubMed: 16339306]

Sohal VS, Zhang F, Yizhar O, and Deisseroth K. (2009). Parvalbumin neurons and gamma rhythms enhance cortical circuit performance. Nature 459, 698–702. [PubMed: 19396159]

Highlights

- Prefrontal VIP interneurons are recruited in the center and open arms of the EPM
- Inhibiting prefrontal VIP interneurons increases open arm exploration
- Inhibiting VIP neurons disrupts mPFC representations of anxiety-related information
- VIP neurons act by disinhibiting theta-band hippocampal-prefrontal communication

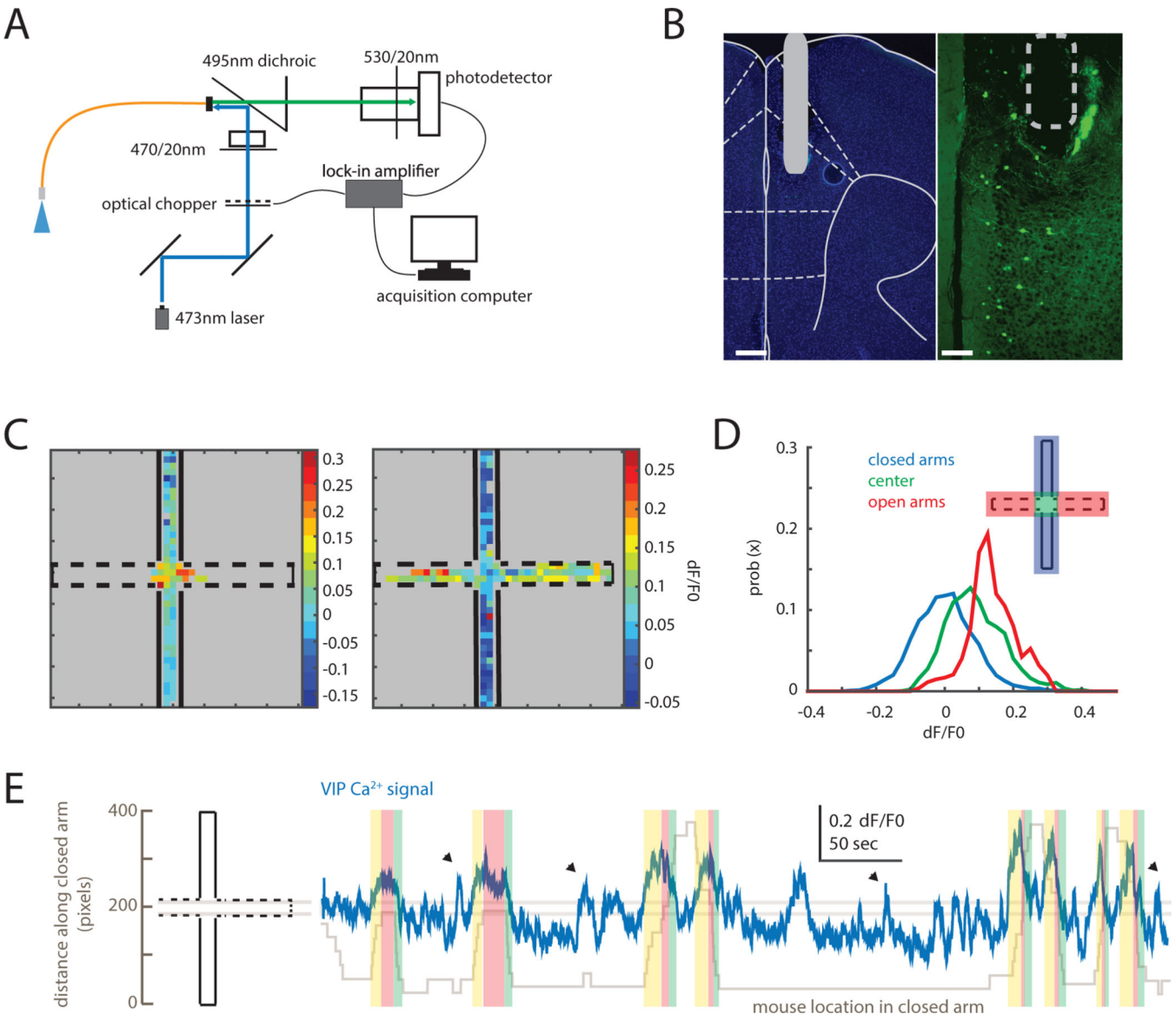

Figure 1. Prefrontal VIP neuron activity reflects elevated plus maze behavior.

(A) Fiber photometry design. An optical fiber delivered 473nm light to mPFC to excite GCaMP6s. GCaMP6s fluorescence was detected and streamed to an acquisition computer using a lock-in amplifier synchronized to an optical chopper.

(B) VIP-Cre mice were injected with AAV-hSyn-FLEX-GCaMP6s. A 400μm optical fiber was implanted with its tip near the prelimbic/infralimbic border (left, DAPI; right, VIP-GCaMP; scale bars: 300 and 90 μm, respectively).

(C) Heatmaps showing the average GCaMP signal from VIP neurons in two individual mice as a function of EPM location. VIP GCaMP signals were highest in the center for a mouse that did not explore the open arms (left); for a mouse that did explore the open arms, VIP GCaMP signals were highest in the open arms (right).

(D) Distributions of VIP-GCaMP signals (dF/F0) in different EPM zones: the closed arms (blue), center zone (green), or open arms (red) (n = 5 mice).

(E) An example trace showing VIP-GCaMP signals during EPM exploration. The VIP-GCaMP signal (blue) is overlaid on top of the position of the mouse along the closed arm axis (gray). Two horizontal lines demarcate the center zone. VIP activity tracks the position of the mouse (yellow, approach towards center zone; red, in center zone; green, exit from center zone). Arrowheads indicate when the mouse was rearing or reorienting within the closed arm.

See also Figures S1 and S2.

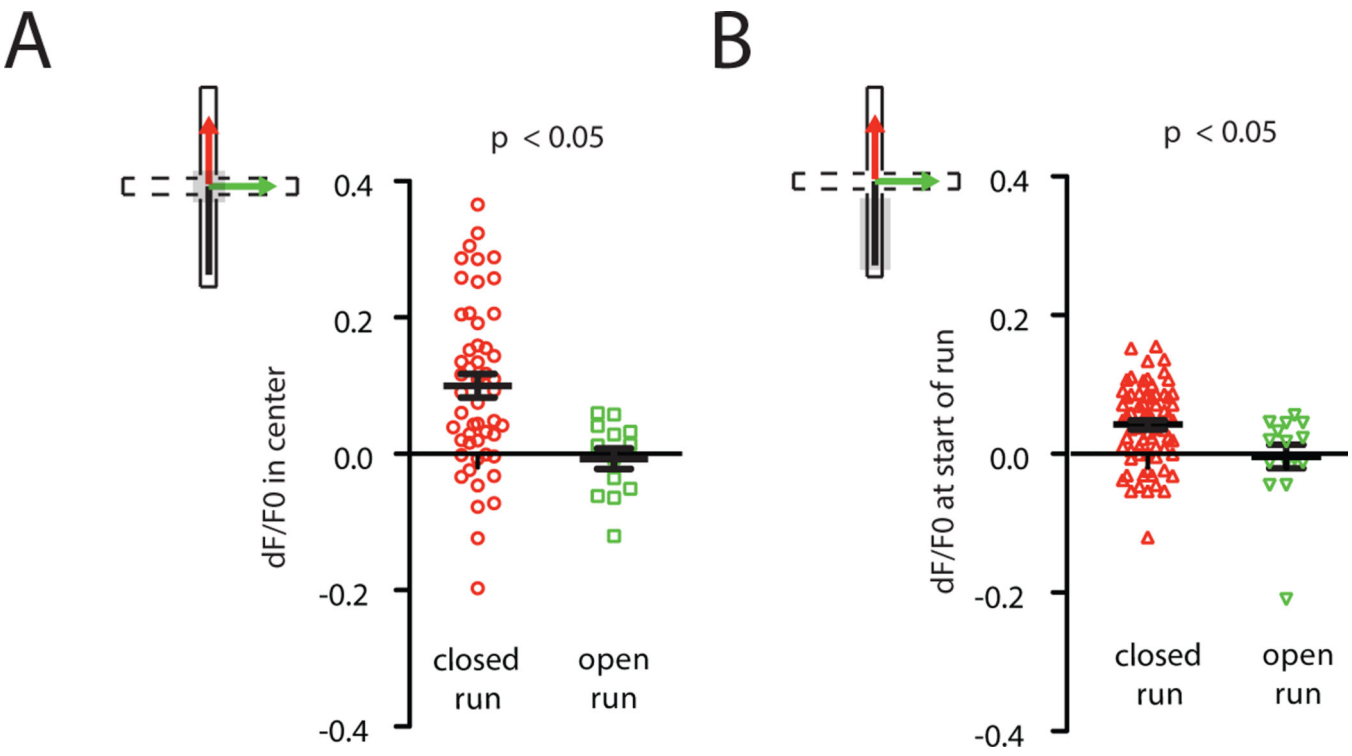

Figure 2. VIP interneurons predict future exploration vs. avoidance.

(A) Average VIP-GCaMP signals in the center zone were lower just prior to runs into the open arms than before runs into the closed arms (ANOVA using mouse and run type as factors; run type: $F_{1,77} = 6.18$, $p = 0.015$; n = 8 mice). Whereas Fig. 1D only includes data from 5 VIP-GCaMP mice run concurrently with PV-GCaMP or SOM-GCaMP mice, this figure includes data from 3 additional VIP-GCaMP mice run subsequently.

(B) Average VIP-GCaMP signals were lower during runs on which mice subsequently entered the open arms compared to those on which mice subsequently entered closed arms (ANOVA using mouse and run type as factors; run type: $F_{1,77} = 4.1$, $p = 0.046$; n = 8 mice).

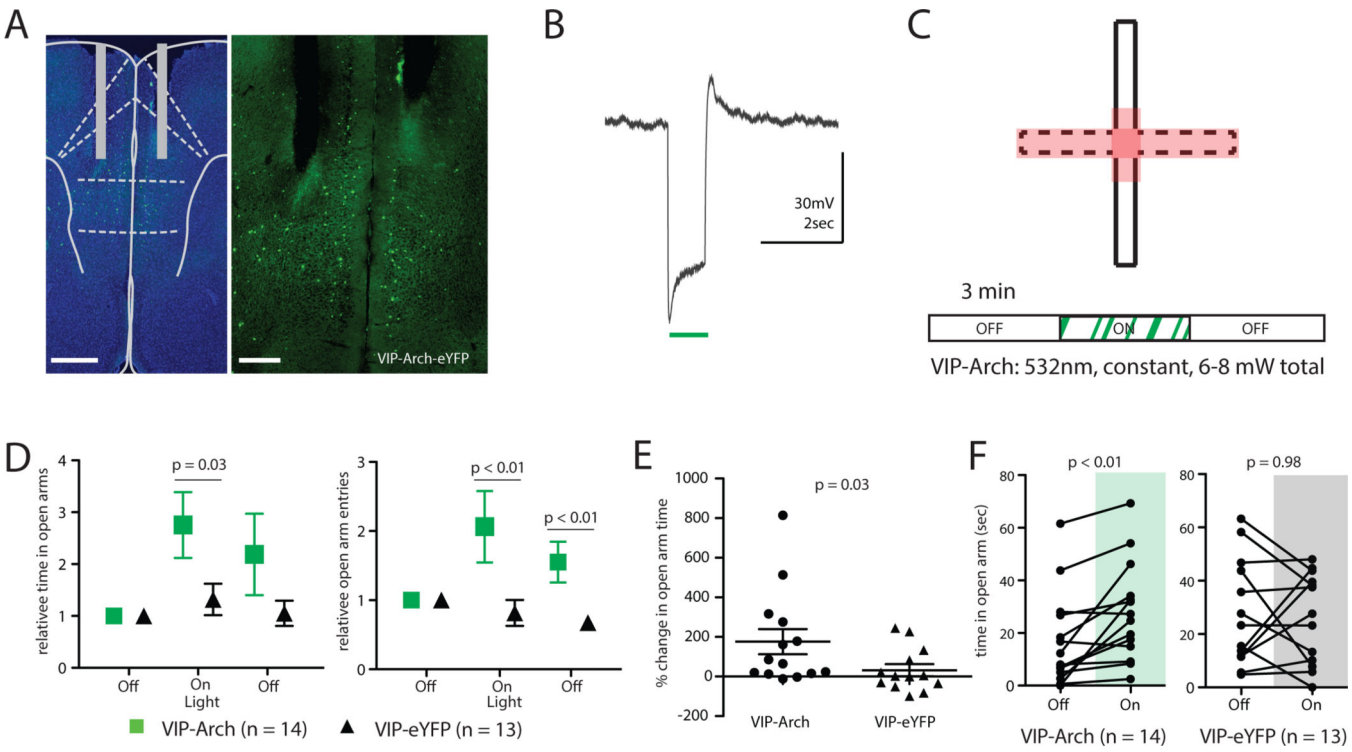

Figure 3. Inhibiting prefrontal VIP neurons increases open arm exploration.

(A) Dual fiber optics were implanted in mPFC near the prelimbic/infralimbic border, in VIP-Cre mice injected with AAV to drive Cre-dependent expression of Arch (scale bars, 500 and 250 μM, respectively).

(B) Example current clamp responses of prefrontal VIP neurons to Arch stimulation using constant 532nm green light (~5mW).

(C) Protocol for “location based” optogenetic stimulation in the EPM. Stimulation (532nm light to activate Arch) was delivered when the mouse entered the stimulation zone (red) during the second 3-minute epoch of EPM exploration.

(D) Inhibiting VIP neurons (green) increased relative open arm time (left) and open arm entries (right) compared to control mice (open arm time: $Z = 2.16$, $^{*}p = 0.03$, rank-sum test; open arm entries: $Z = 2.69$, $^{**}p < 0.01$, rank-sum test). Open arm time and entries were normalized to the first 3-minute epoch of EPM exploration.

(E) During the period of light stimulation, VIP-Arch mice increase the absolute time spent in the open arms more than VIP-eYFP mice ($Z = 2.16$, $^{*}p < 0.05$, rank-sum test).

(F) Delivering light to activate Arch (green) increased time spent in the open arm, compared to the first 3 minutes of EPM exploration (when no light was delivered), for VIP-Arch mice ($Z = -2.98$, $p = 0.003$, signed-rank test, $n = 14$) but not for VIP-eYFP controls ($Z = -0.04$, $p = 0.98$, signed-rank test, $n = 13$).

See also Figure S3.

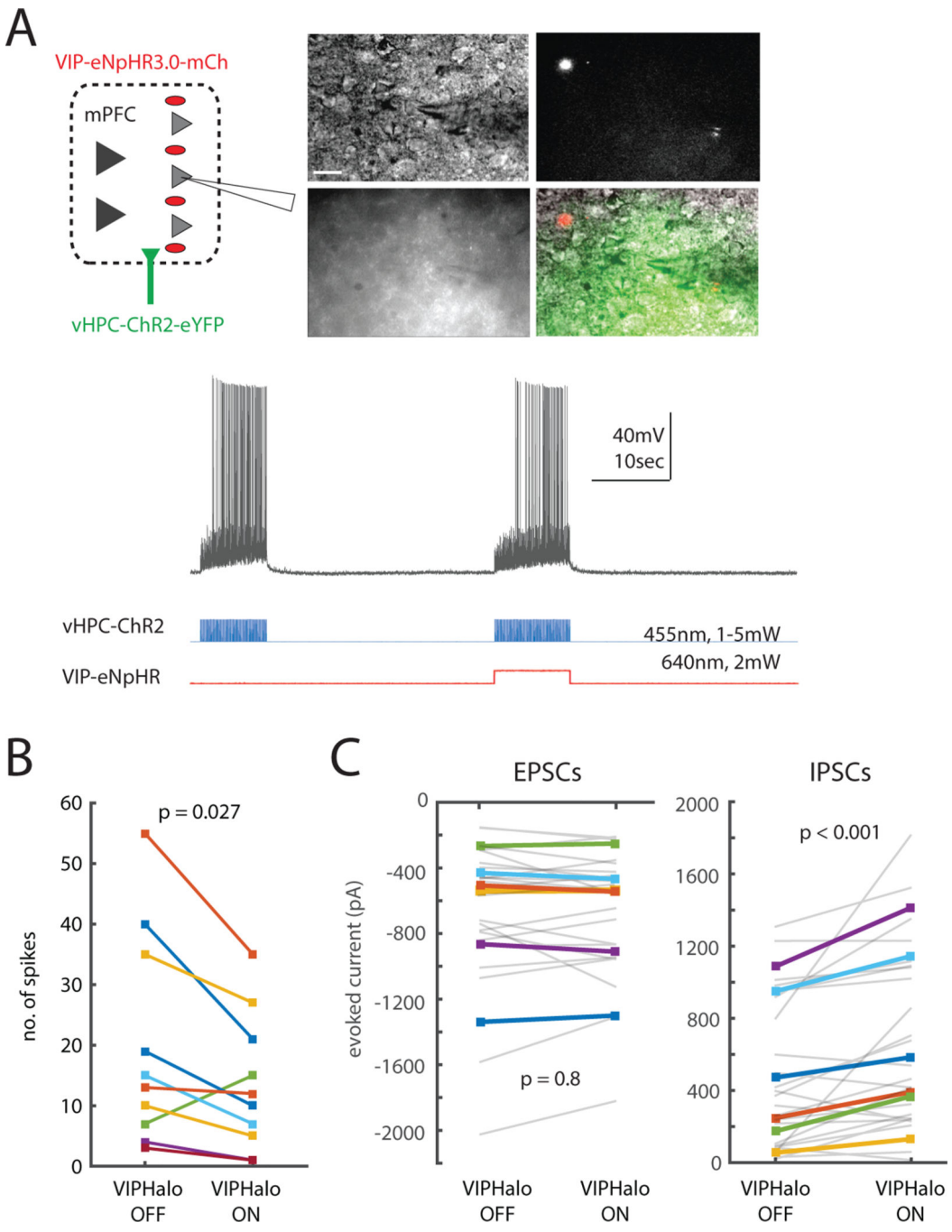

Figure 4. VIP interneurons disinhibit prefrontal responses to hippocampal inputs.

(A) Top, left: Experimental design for in vitro patch clamp experiments. We recorded from layer 2/3 mPFC neurons in VIP-eNpHR mice co-injected with CaMKII-ChR2 in vHPC. **Top, right:** representative DIC and fluorescence images. For recordings, we specifically targeted visually identified layer 2/3 pyramidal neurons near eYFP-tagged vHPC terminals (yellow-green) and mCherry-tagged VIP-eNpHR neurons (red) (scale bar, 15 p,m). **Bottom:** We stimulated ChR2 in vHPC terminals at 10Hz +/− 10 sec of concurrent VIP-eNpHR stimulation (constant light, 640nm, 2mW).

(B) Inhibiting mPFC VIP interneurons reduced L2/3 pyramidal neuron spiking in response to vHPC terminal stimulation ($p = 0.027$, $n = 10$ cells, sign-rank test).
(C) Inhibiting VIP neurons increased evoked IPSCs (right) but had no effect on evoked EPSCs (left) ($p < 0.001$ and $p = 0.8$, respectively, $n = 6$ cells; ANOVA using cell ID, inhibition, and sweep as factors; $F_{1,38} = 13.2$). EPSCs and IPSCs were measured by recording peak inward or outward currents in voltage clamp at −70 mV or +10 mV, respectively. Each gray line represents data from a single trace (we recorded three times from each cell), and each colored line represents the average of the three traces from a single cell. The same color indicates the same cell in the left and right panels (different cells were used for panel B and this panel).
See also Figure S4.

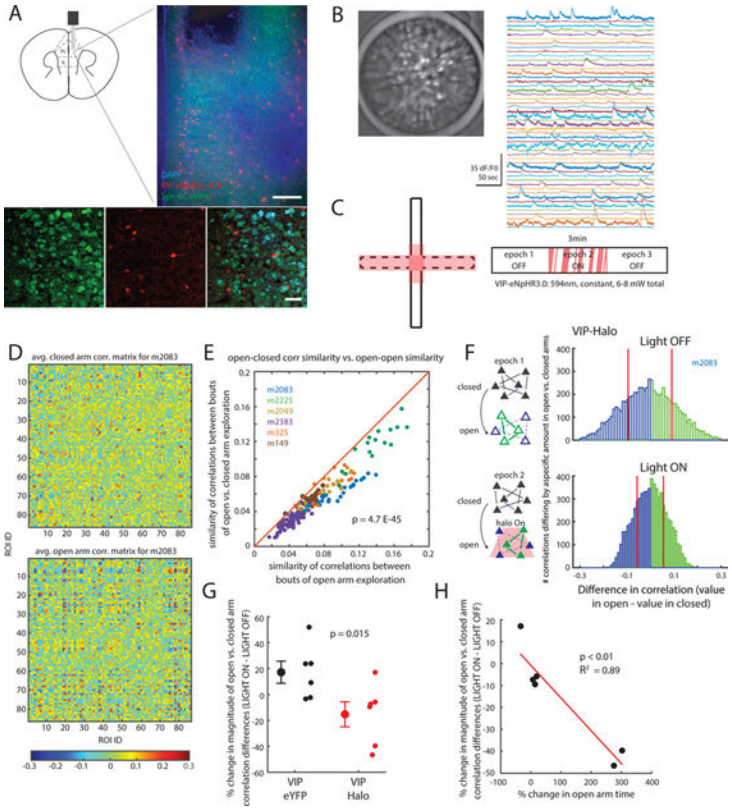

Figure 5. Inhibiting VIP neurons attenuates anxiety-driven changes in patterns of mPFC microcircuit activity.

(A) A 500um diameter GRIN lens was implanted in the mPFC of VIP-Cre mice injected with AAV-DIO-eNpHR3.0-mCh to express eNpHR in VIP neurons, and AAV-Syn-GCaMP6m to express GCaMP. The GRIN lens tip was in ventral PL cortex (scale bars, 90 and 50 μm, respectively).

(B) Representative GCaMP signals. Max-projected Z-stack (1000 frames; 50 sec) of Syn-GCaMP6m-infected cells in mPFC (left) and signals from putative cells detected using PCA/ICA (right).

(C) Experimental design. Optogenetic inhibition (594nm, 6–8mW total) was triggered when the mouse entered the stimulation zone (red shading) during the second 3min epoch of EPM exploration.

(D) Averaged correlation matrices representing example patterns of microcircuit activity in the closed vs. open arms. 20 correlation matrices (from one mouse) were averaged for randomly selected times corresponding to closed (top) or open (bottom) arm exploration.

(E) Similarity of correlation matrices in open arms to those in the closed arms. For each correlation matrix, based on 2.5 sec of open arm exploration, we computed the similarity between that matrix and other matrices corresponding to exploration of either closed (y-axis) or open (x-axis) arms. Every point falls below the unity line, indicating that all open arm correlation matrices were more similar to other open arm matrices, than to closed arm matrices ($p < 10^{-45}$, paired t-test). Different colors indicate data from different mice (n = 6 mice).

(F) The distribution of correlations (from one mouse) which exhibit significant ($p < 0.01$) increases (green) or decreases (blue) between the closed and open arms is shown for the first or second 3 min epoch of EPM exploration (top: first epoch / no VIP interneuron inhibition; bottom: second epoch / VIP interneurons are inhibited in the stim zone). The magnitude of significant changes in correlations between the closed and open arms is reduced during the second epoch, i.e., when VIP interneurons are inhibited. For each epoch, red vertical lines indicate the mean magnitude of significant increases or decreases in correlations.

(G) The magnitude of significant changes in correlations between the closed and open arms is reduced when we deliver light to mice which express eNpHR in VIP interneurons, but not when we deliver light to control (eNpHR-negative) mice ($p = 0.015$, rank-sum test, $n = 6$ mice in each cohort).

(H) The amount by which inhibiting VIP interneurons suppresses changes in correlations between the open and closed arms predicts the degree to which optogenetically inhibiting VIP interneurons increases open arm exploration ($p < 0.01$, $R^2 = 0.89$; $n = 6$ mice).

See also Figure S4.

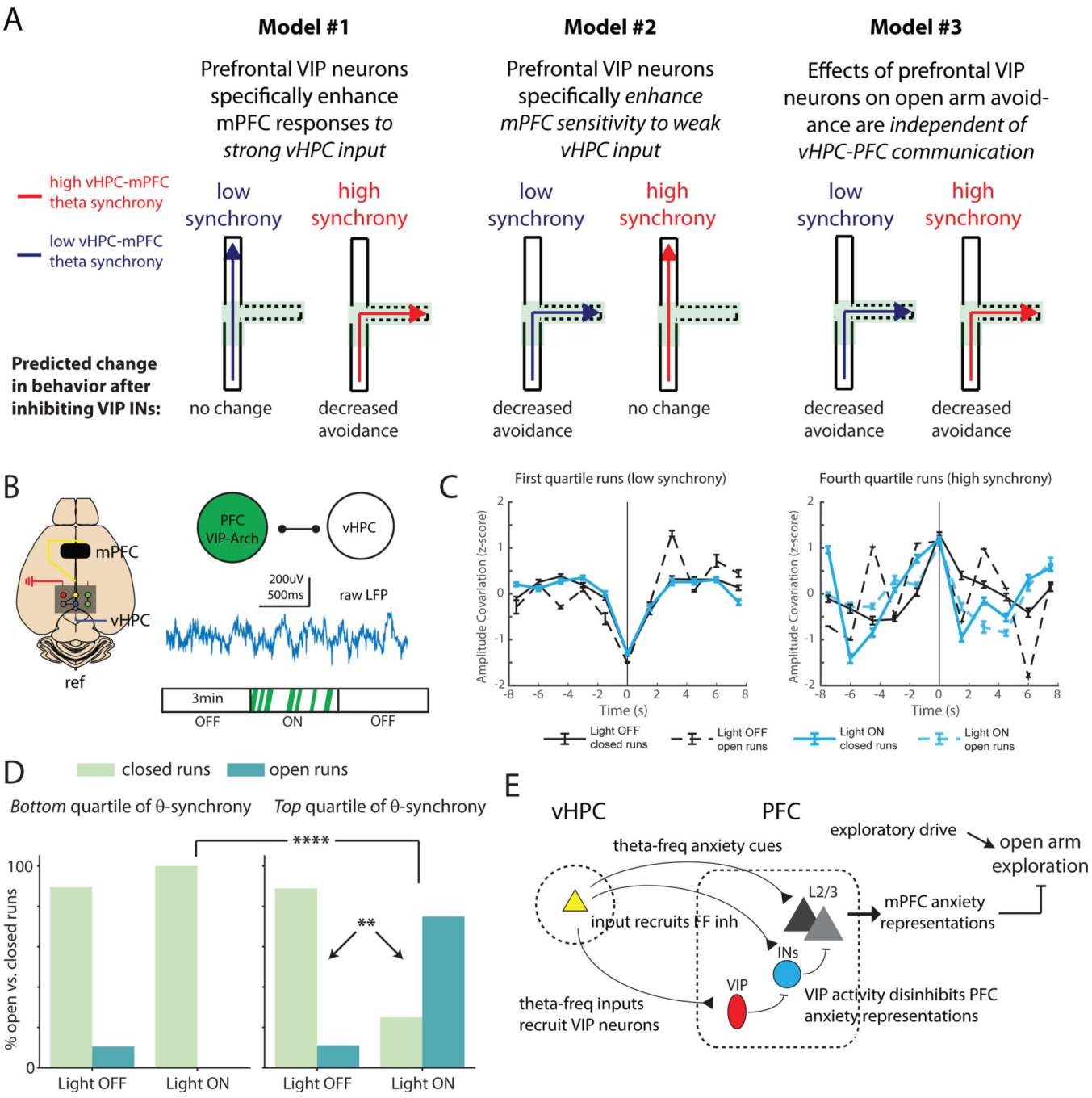

Figure 6. Inhibiting prefrontal VIP neurons selectively enhances open arm exploration when hippocampal-prefrontal theta-synchrony is relatively high.

(A) Schematic: different models for how the effect of inhibiting VIP interneurons (decreased open arm avoidance) might depend on the current state of the vHPC-mPFC network. Blue and red trajectories represent behavior when vHPC-mPFC theta synchrony is low or high, respectively, corresponding to periods of weak vs. strong vHPC-mPFC communication. Trajectories enter the center compartment of the EPM, then either avoid the open arms (dotted lines) and return to a closed compartment (solid lines), indicating no change in normal avoidance behavior, or explore the open arms, indicating decreased avoidance.

(B) Experimental design. Local field potentials were recorded from electrodes in mPFC and vHPC of VIP-Arch mice implanted with bilateral mPFC optical fibers during the real-time EPM optogenetic assay.

(C) For mice expressing Arch in mPFC VIP interneurons (n = 4), we identified runs into the stimulation zone for which the vHPC-mPFC synchrony (amplitude covariation) as mice entered the stim-zone (z-scored relative to the rest of the run, i.e., +/− 7.5 sec from stim-zone entry) was either low (left) or high (right), i.e., in the bottom or top quartile at t=0 (time of stim-zone entry), respectively. Amplitude was calculated from the theta-filtered LFP signal.

(D) For runs in each quartile (left: low theta synchrony, right: high theta synchrony), we computed the fraction which either avoided the open arms ("closed" runs, light green bars) or explored the open arms ("open" runs, teal bars). We performed this analysis separately for periods during which no light was delivered ("OFF") and periods during which light (to trigger optogenetic inhibition) was selectively delivered in the stimulation zone ("ON"). When light is ON, the proportion of trials with relatively high synchrony at the time of stim-zone entry which explore the open arms is significantly increased, selectively for high synchrony trials (χ^2 test; $p = 0.008$ for the number of open vs. closed runs during high synchrony trials with light ON vs. OFF; $p = 0.0006$ for the number of open vs. closed arm runs for high vs. low synchrony trials with light ON). ** $p < 0.01$, **** $p < 0.0001$.

(E) Schematic: When vHPC-mPFC theta synchrony is high, theta-frequency vHPC input recruits prefrontal VIP interneuron-mediated disinhibition, enhancing prefrontal anxiety representations. (The blue circle represents non-VIP interneurons in mPFC). These prefrontal anxiety representations inhibit open arm exploration. Inhibiting prefrontal VIP interneurons would increased feedforward inhibition, disrupting the ability of vHPC input to drive prefrontal anxiety representations which normally inhibit open arm exploration. The net effect would be to increase open arm exploration during periods when such exploration is normally prevented by hippocampal-prefrontal communication.

See also Figure S5 and Table S1.